A

	grade 1or 2	grade 3 or 4
PHLDA3 LOH +	10	21
PHLDA3 LOH-	11	3

(p<0.01, Fisher's exact test)

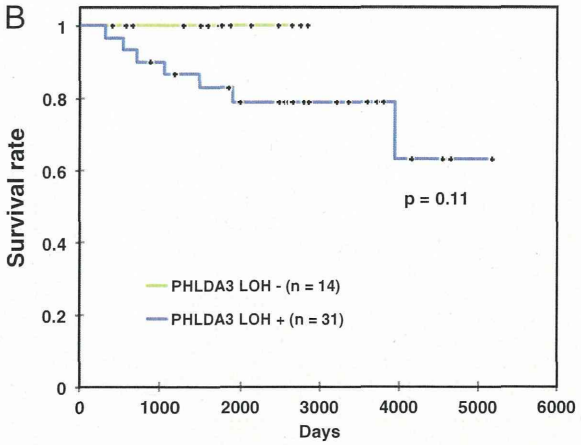

C

	grade 1or 2	grade 3 or 4
MEN1 LOH +	19	19
MEN1 LOH-	4	3

(p=0.73, Fisher's exact test)

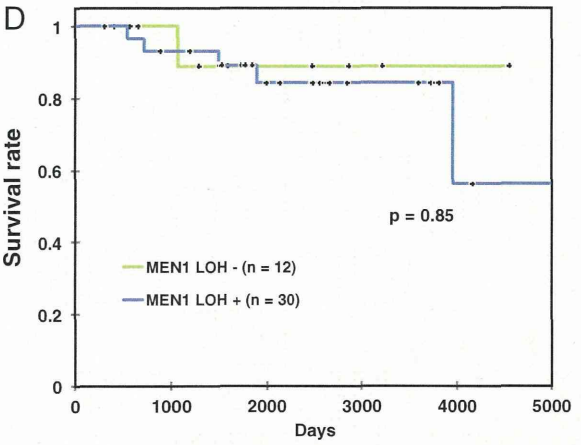

Fig. 3. LOH at the *PHLDA3* and *MEN1* gene locus and progression of PanNETs. (*A*) LOH at the *PHLDA3* gene locus and grade of PanNETs. The *P* value was calculated by Fisher's exact test. (*B*) Kaplan–Meier plots of overall survival of patients with PanNETs. Fourteen or 31 patients without or with *PHLDA3* LOH were analyzed. Wilcoxon test was used to determine the *P* value. (*C*) LOH at the *MEN1* gene locus and grade of PanNETs. (*D*) Kaplan–Meier plot for overall survival of patients with PanNETs. Twelve or 30 patients without or with *MEN1* LOH were analyzed as in *B*.

enhanced expression of *PHLDA3* in a 5-aza-C concentration-dependent manner. A similar result was obtained using a human PanNET cell line A99 (Fig. 4*F*) and the mouse insulinoma cell line MIN6 that has very low PHLDA3 expression (*SI Appendix*, Fig. S3 *A* and *B*). These results indicate that methylation of the *PHLDA3* gene affects *PHLDA3* transcription levels. We then analyzed the methylation status of the *PHLDA3* promoter in PanNET samples that had undergone LOH at the *PHLDA3* locus. As shown in Fig. 4*G*, methylation was not detected in normal pancreas or islets, whereas significant methylation was detected in all LOH+ samples (seven of seven) analyzed. These results show that the *PHLDA3* gene can undergo methylation in addition to LOH in PanNETs, indicating that a two-hit inactivation of the *PHLDA3* gene may often occur. We also analyzed LOH– samples and found detectable levels of methylation in two of four samples (*SI Appendix*, Fig. S4). Thus, the repression of *PHLDA3* expression in LOH– samples due to methylation may also contribute to tumor progression in PanNETs.

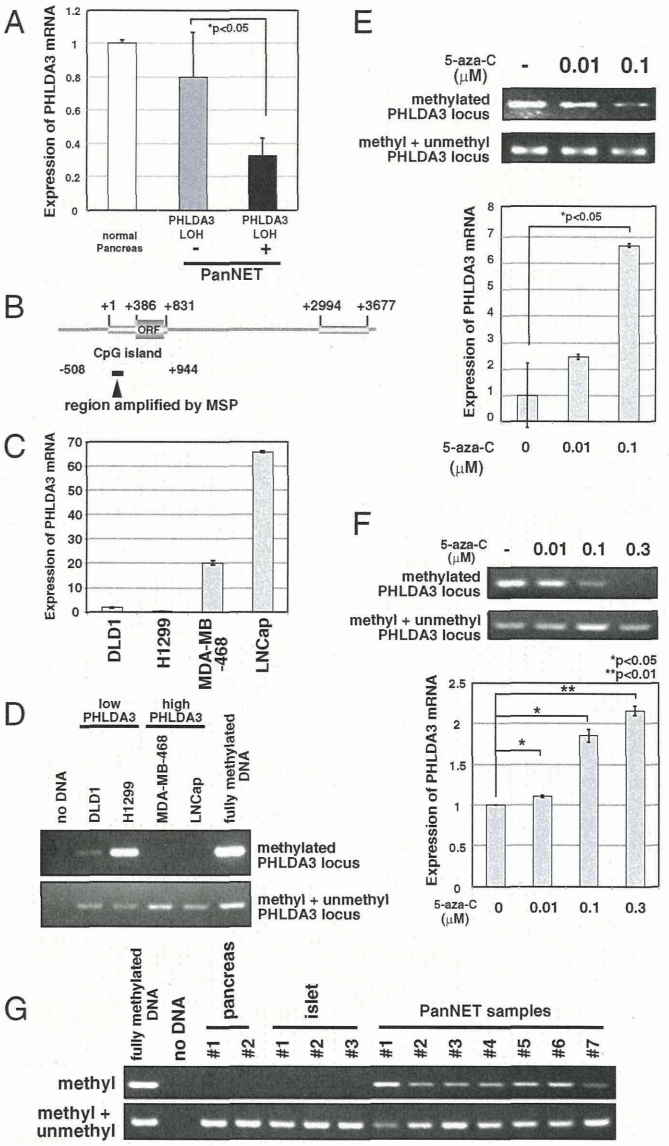

Fig. 4. *PHLDA3* expression and promoter region methylation status in PanNETs. (*A*) *PHLDA3* gene expression in PanNETs. Total RNAs were prepared from normal pancreas and PanNETs. RNA was pooled from 5 normal pancreases for the normal controls. RNA was isolated from PanNET samples with (10 samples) or without LOH (7 samples). Gene expression was quantitated by RT-PCR and normalized to *GAPDH*. (*B*) Genomic organization of *PHLDA3* promoter region and location of CpG island. Wide lines indicate exonic regions of the *PHLDA3* gene (+1 to +831 and +2994 to +3677). (*C*) *PHLDA3* gene expression in cell lines. Gene expression was analyzed as in *A*. (*D*) DNA methylation of the *PHLDA3* promoter. Genomic DNAs from the indicated cell lines were analyzed by methylation-specific PCR. Positions of the primers used in the assay are shown in *B*. Primers designed to amplify methylated DNA (upper panel) or DNA with or without DNA methylation (lower panel) were used. Fully methylated DNA was used as a control. (*E* and *F*) 5-aza-C treatment of Lung NET H1299 cells (*E*) or PanNET A99 cells (*F*). Both genomic DNAs and total RNAs were isolated, and analyzed as in *D* and *A*, respectively. (*G*) Methylation status of *PHLDA3* promoter in normal pancreas, normal isolated islets and PanNETs (samples showing LOH at the *PHLDA3* locus was analyzed). Genomic DNAs were prepared and analyzed as in *D*.

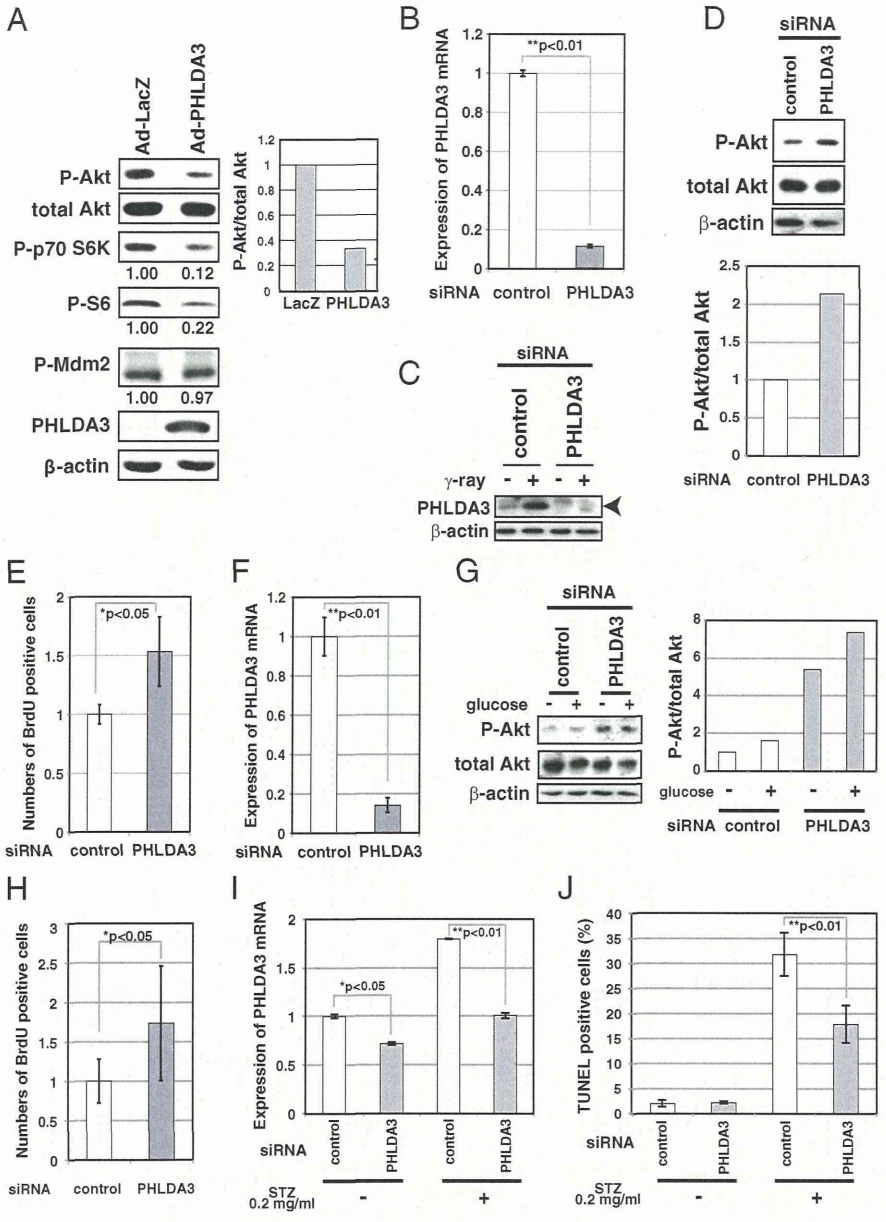

Fig. 5. Effect of PHLDA3 expression on Akt activity, cell proliferation and apoptosis of islet cells. (*A*) Effect of PHLDA3 expression on Akt activity in MIN6 cells. MIN6 cells were transduced with Ad-LacZ or Ad-PHLDA3 at a moi of 35, and harvested 30 h post-infection. Akt activation and phosphorylation of Akt downstream signaling molecules were analyzed by Western blotting and quantified by normalization to total Akt levels (P-Akt) or by β-actin levels (P-p70 S6K, P-S6, P-Mdm2). (*B* and *C*) Efficiency of siRNA inhibition of PHLDA3 expression in RIN cells. RIN cells were transfected with control or PHLDA3 siRNAs. *PHLDA3* mRNA levels were analyzed 31 h posttransfection by quantitative RT-PCR, standardized against β-actin (*B*). PHLDA3 protein levels were also determined 48 h posttransfection by Western blotting (*C*), using cells subjected to γ-ray irradiation (20 Gy) versus untreated. The γ-ray irradiated samples were included to help identify the band representing PHLDA3 protein (PHLDA3 is induced by p53 activation). (*D*) Effect of PHLDA3 expression on Akt activation in RIN cells. RIN cells were transfected as in *B* and Akt activation was analyzed by Western blotting 31 h posttransfection (left) and quantified by normalization to total Akt levels (right). (*E*) Effect of PHLDA3 expression on RIN cell proliferation. RIN cells were transfected as in *B*, and labeled with BrdU for 3 h and harvested 28 h post transfection. BrdU positive cells were quantified by using Ziva Ultrasensitive BrdU assay. (*F*) siRNA suppression of *PHLDA3* expression in primary islet cells. Isolated primary islet cells were transfected with control or PHLDA3 siRNA, harvested 30 h post transfection, and *PHLDA3* mRNA levels were analyzed by quantitative RT-PCR as in *B*. (*G*) Effect of PHLDA3 expression on Akt activation in primary islet cells. Cells were transfected with siRNA as in *F* and 48 h post-transfection were treated with glucose (30 mM) for 20 min. Levels of Akt activation were analyzed as in *D*. (*H*) Effect of PHLDA3 expression on primary islet cell proliferation. Cells were transfected as in *F*, labeled with BrdU for 4 h and harvested 30 h post transfection. BrdU positive cells were analyzed as in *E*. (*I* and *J*) Effect of PHLDA3 expression on STZ-induced apoptosis of primary rat islets. Isolated islets were pooled from three rats, and transfected with control or PHLDA3 siRNA. At 75 h posttransfection, islets were treated with STZ (20 μg/mL) for 30 min. Islets were then cultured overnight, and total RNAs were prepared and *PHLDA3* expression was analyzed by quantitative RT-PCR as in B (*I*), or subjected to TUNEL staining and analyzed by FACS (*J*).

PHLDA3 Controls Akt Activity, Cell Proliferation, and Apoptosis of Islet Cells. PanNETs are derived from pancreatic islet endocrine cells. It is well known that, in islet β cells, Akt signaling plays a central role in promoting cell growth and inhibiting apoptosis (5). Therefore, in β cells, loss of PHLDA3 function may result in the hyperactivation of Akt oncogenic signaling, and thus lead to tumor progression. To analyze the function of PHLDA3 in islet β cells, we examined RIN and MIN6 cells, cell lines derived from pancreatic β cells (Fig. 5 *A–E*). Whereas RIN cells have detectable levels of PHLDA3 expression, MIN6 has very low PHLDA3 expression (*SI Appendix*, Fig. S3*A*). We first used a gain-of-function approach to confirm that PHLDA3 functions as a repressor of Akt in MIN6 cells. As shown in Fig. 5*A*, expression of PHLDA3 resulted in decreased Akt activation levels and decreased phosphorylation of signaling molecules downstream of Akt. Similar results were obtained using *PHLDA3*$^{-/-}$ mouse embryonic fibroblasts (MEFs, *SI Appendix*, Fig. S5). Next, we knocked down PHLDA3 expression in RIN cells using siRNA against PHLDA3 (Fig. 5 *B* and *C*), and observed increased Akt activation and cell proliferation (Fig. 5 *D* and *E*). We observed similar results in normal primary rat islet cells, i.e., knockdown of PHLDA3 expression resulted in activation of Akt (with or without glucose stimulation) and significant enhancement of cell proliferation (Fig. 5 *F–H* and *SI Appendix*, Fig. S6). Next, we analyzed the effect of PHLDA3 expression on the apoptosis of islet cells induced by Streptozotocin (STZ), a chemical that is particularly toxic to insulin-producing β cells (14). We observed that although inhibition of *PHLDA3* expression by siRNA was relatively poor in isolated rat islets (Fig. 5*I*), this knockdown significantly reduced the number of apoptotic cells caused by STZ treatment (Fig. 5*J*). Collectively, these results demonstrate that PHLDA3 controls Akt activity, cell growth, and the apoptosis of islet cells.

Development of Hyperplastic Islets in *PHLDA3*-Deficient Mice. To analyze the effect of PHLDA3 deficiency on islets in vivo, we examined the pancreases of *PHLDA3*-deficient mice. Differences in islet sizes were not detected in 3-mo-old *PHLDA3*$^{+/+}$ or *PHLDA3*$^{-/-}$ mice (*SI Appendix*, Fig. S7). However, in 6-mo-old *PHLDA3*$^{-/-}$ mice, we found significantly fewer islets that were smaller than 0.01 mm^2 and significantly more islets that were larger than 0.01 mm^2, compared with *PHLDA3*$^{+/+}$ mice (Fig. 6 *A* and *C*).

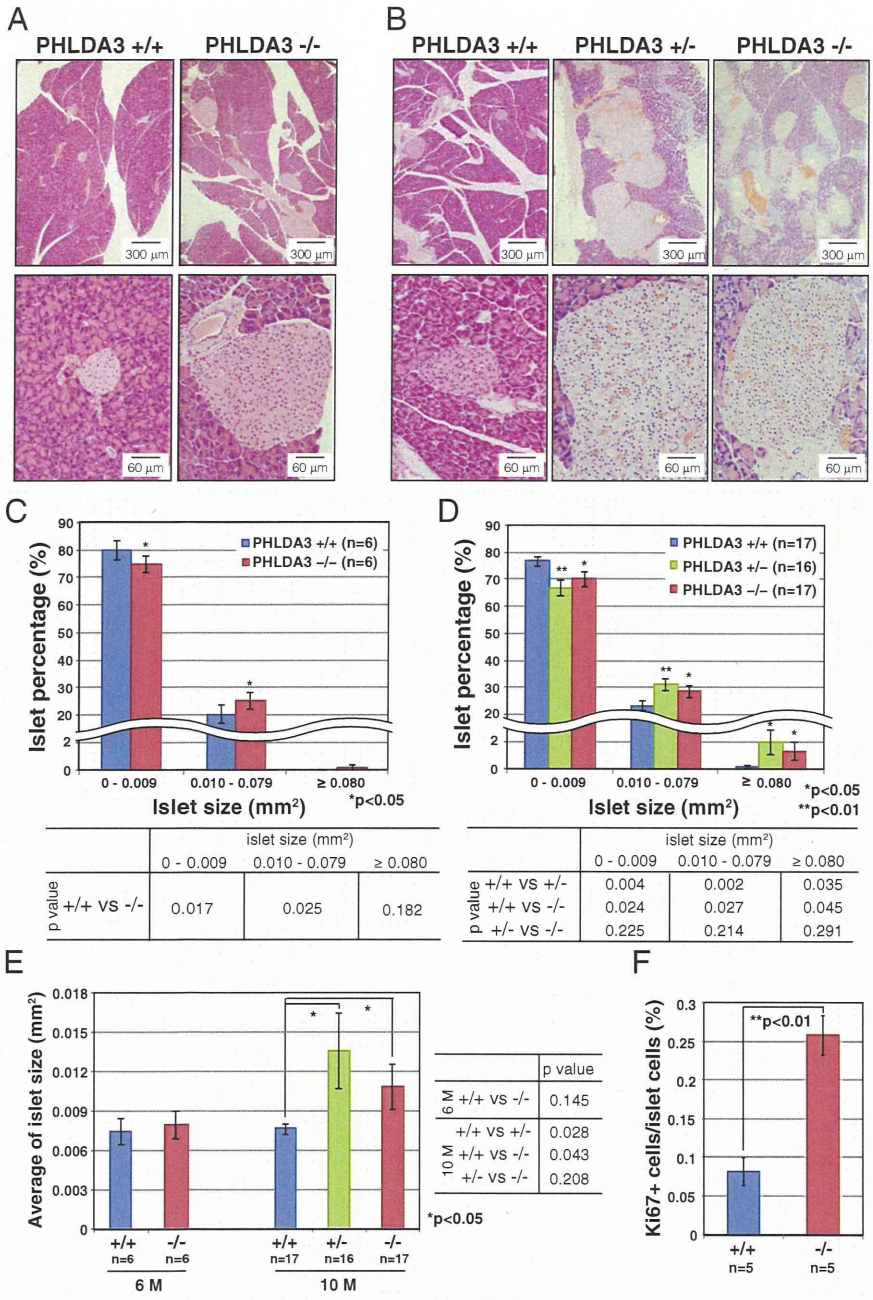

	islet size (mm²)		
	0 - 0.009	0.010 - 0.079	≥ 0.080
p value +/+ vs -/-	0.017	0.025	0.182

	islet size (mm²)		
	0 - 0.009	0.010 - 0.079	≥ 0.080
p value +/+ vs +/-	0.004	0.002	0.035
+/+ vs -/-	0.024	0.027	0.045
+/- vs -/-	0.225	0.214	0.291

		p value
6 M	+/+ vs -/-	0.145
10 M	+/+ vs +/-	0.028
	+/+ vs -/-	0.043
	+/- vs -/-	0.208

Fig. 6. Hyperplastic islets in *PHLDA3*-deficient mice. Six-month-old (21- to 31-wk-old) (*A*, *C*, and *E*) and 10-mo-old (39- to 49-wk-old) (*B* and *D*–*F*) mice were analyzed. (*A* and *B*) Hematoxylin and eosin staining of islets from wild-type, heterozygote and *PHLDA3*-deficient mice (*A*, 6-mo; *B*, 10-mo). (*C*–*E*) Calculation of islet sizes. Islet areas were calculated from hematoxylin and eosin-stained pancreas sections. One (6-mo-old mice) or three pancreas sections (10-mo-old mice; sections separated by more than 20 μm *z* axis) were analyzed per mouse. Islet areas from indicated numbers (n) of mice were analyzed. Size distributions of islets (*C*, 6-mo; *D*, 10-mo) and average islet sizes (*E*; 6- and 10-mo-old) are shown. The *P* values between $PHLDA3^{+/+}$ and $PHLDA3^{+/-}$ or $PHLDA3^{-/-}$ were calculated and are shown (*$P < 0.05$; **$P < 0.01$). (*F*) Quantitation of Ki67-positive cells. Pancreas sections from indicated numbers (n) of mice were analyzed. Islet nuclei number and Ki67-positive nuclei number were counted and the percentage of Ki67-positive cells was calculated. (**$P < 0.01$) Representative images are shown in *SI Appendix*, Fig. S4.

However, the overall average islet size at 6 mo was not significantly different between $PHLDA3^{+/+}$ and $PHLDA3^{-/-}$ mice (Fig. 6*E*). At 10 mo, abnormally large islets (larger than 0.08 mm^2) were frequently found (Fig. 6 *B* and *D*), and the average islet sizes were significantly larger in 10-mo-old $PHLDA3^{+/-}$ and $PHLDA3^{-/-}$ mice compared with $PHLDA3^{+/+}$ mice (Fig. 6*E*). Thus, a difference in islet sizes between $PHLDA3^{+/+}$ and $PHLDA3^{-/-}$ mice appears to emerge between 3 and 10 mo of age. We stained the islets with Ki67 antibody and found significantly more Ki67-positive cells in $PHLDA3^{-/-}$ islets compared with the $PHLDA3^{+/+}$ islets (Fig. 6*F*; representative images are shown in *SI Appendix*, Fig. S8). These data show that loss of PHLDA3 expression results in enhanced proliferation of islet cells.

Enhanced Proliferation of β Cells and Altered Glucose Metabolism in *PHLDA3*-Deficient Mice. The islets were further stained with anti-insulin and anti-glucagon antibodies to determine the numbers of β and α cells, respectively, within the islets. Normal murine islets have β cells in the center of the islet and α cells at the periphery surrounding the β cells (as shown in $PHLDA3^{+/+}$ islets in Fig. 7*A*). However, in the hyperplastic islets of $PHLDA3^{+/-}$ and $PHLDA3^{-/-}$ mice, huge numbers of β cells and relatively small numbers of α cells were often observed, and the hyperplastic islets often showed abnormal islet architecture, with few α cells at the periphery of the islets (Fig. 7*A*). We calculated the areas occupied by α and β cell types to determine which of these had increased. As shown in Fig. 7*B*, the mean percentage area occupied by β cells was significantly higher in $PHLDA3^{-/-}$ islets. The area occupied by β cells was also significantly high in large $PHLDA3^{-/-}$ islets (larger than 0.05 mm^2) compared with that seen in large islets infrequently found in $PHLDA3^{+/+}$ mice (Fig. 7*B*). Because we had found a significantly higher number of proliferating cells in $PHLDA3^{-/-}$ islets (Fig. 6*F*), we stained the islets with anti-Ki67, -insulin, and -glucagon antibodies to identify which cell types within the islets were proliferating. As shown in Fig. 7*C*, we found that most Ki67-

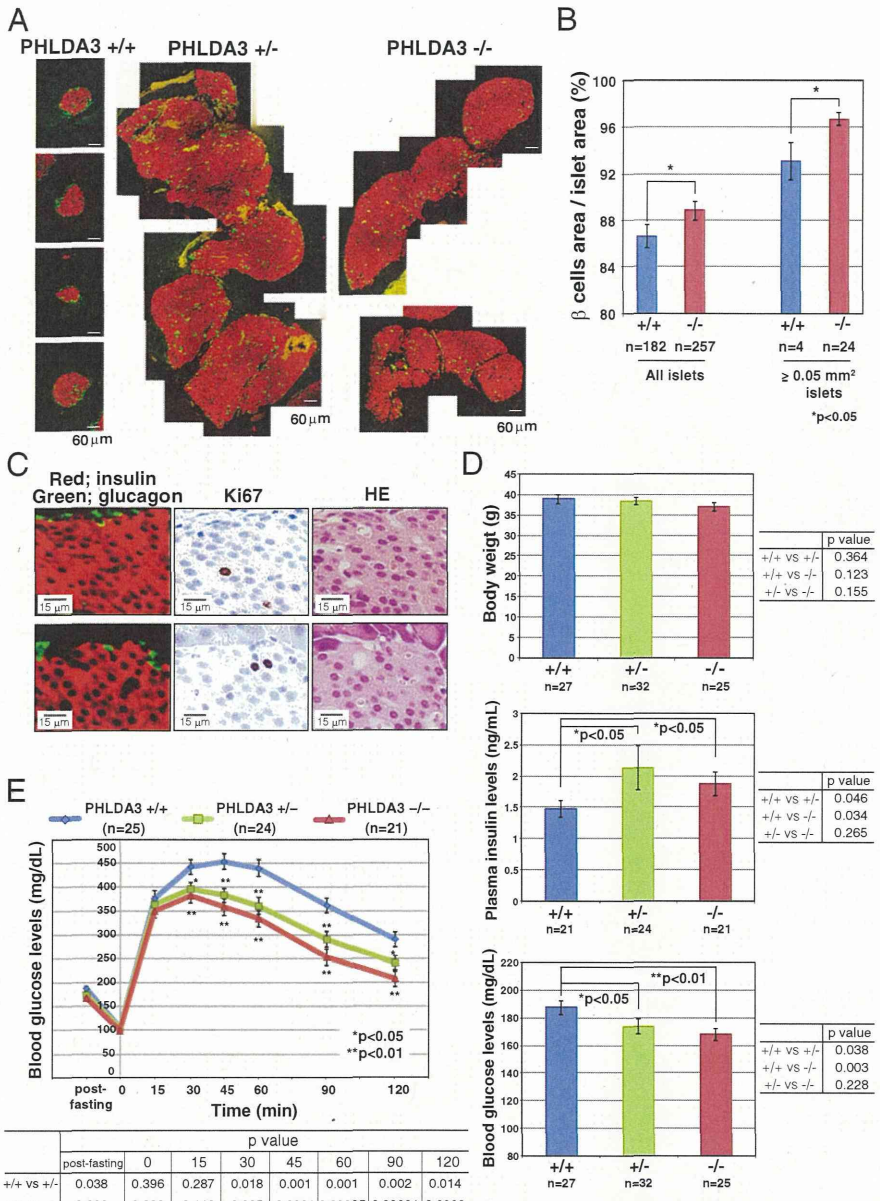

Fig. 7. Proliferation of β cells in the islets of *PHLDA3*-deficient mice. Ten-mo-old (39- to 49-wk-old) mice were analyzed. (*A*) Distribution of β and α cells in pancreas sections. Pancreas sections were stained with antibodies to identify β cells (anti-insulin; red) and α cells (anti-glucagon; green). Representative images of hyperplastic islets from *PHLDA3*$^{+/-}$ and *PHLDA3*$^{-/-}$ mice are shown. (*B*) Percent area occupied by β cells. Pancreas sections were stained as in *A*, and areas occupied by α- and β-cells in indicated numbers of islets from *PHLDA3*$^{+/+}$ (five mice were analyzed) and *PHLDA3*$^{-/-}$ (six mice were analyzed) were calculated and percentages of β-cell areas in the islets were determined. Semihyperplasic islets and hyperplastic islets (larger than 0.05 mm^2 islet area) were separately calculated and shown at the right. (*$P < 0.05$; **$P < 0.01$). (*C*) Proliferation in pancreas sections. Serial pancreas sections of *PHLDA3*$^{-/-}$ mice were stained with anti-insulin and anti-glucagon, anti-Ki67 and HE, to determine the cell types that are Ki67 positive. Representative images are shown. (*D*) Body weight, blood glucose and insulin levels. Indicated numbers (n) of mice were analyzed. Plasma insulin levels and blood glucose levels were determined in blood from tail vein samples, and were determined twice for each mouse. Mice were fed ad libitum. (*$P < 0.05$; **$P < 0.01$). (*E*) Glucose tolerance test (GTT). Indicated numbers (n) of overnight-fasted mice were subjected to GTT by i.p. injection of glucose (2 mg/g body weight). GTT was performed twice for each mouse. The *P* values between *PHLDA3*$^{+/+}$ and *PHLDA3*$^{+/-}$ or *PHLDA3*$^{-/-}$ were calculated and are shown in the panels (*$P < 0.05$; **$P < 0.01$). The differences between *PHLDA3*$^{+/-}$ and *PHLDA3*$^{-/-}$ were not significant ($P > 0.05$).

positive cells were β cells in *PHLDA3*$^{-/-}$ islets. Taken together, these data show that islet β cell proliferation is enhanced in *PHLDA3*-deficient islets.

It would be expected that abnormal proliferation of β cells would result in the excess production of insulin, leading to altered glucose metabolism in *PHLDA3*-deficient mice. As shown in Fig. 7*D*, although the *PHLDA3* genotype had no influence on body weights, 10-mo-old *PHLDA3*$^{+/-}$ and *PHLDA3*$^{-/-}$ mice had higher plasma insulin and lower blood glucose levels compared with age-matched wild-type mice under fed conditions. Similar results were obtained in 6-mo-old fed mice (*SI Appendix*, Fig. S9*A*) and in 10-mo-old fasted mice (*SI Appendix*, Fig. S9*B*). Therefore, we performed glucose tolerance tests and found significant enhancement of glucose tolerance in *PHLDA3*$^{+/-}$ and *PHLDA3*$^{-/-}$ mice (Fig. 7*E*). These data show that loss of PHLDA3 expression results in enhanced proliferation of islet cells, especially β cells, and consequential increase of insulin secretion.

We further characterized *PHLDA3*$^{-/-}$ islets using several β cell markers: the endocrine cell marker chromogranin A (*SI Appendix*, Fig. S10), the β cell differentiation marker Glut2 (*SI Appendix*, Fig. S11), and deposition of IAPP (islet amyloid polypeptide; *SI Appendix*, Fig. S12). None of these markers showed significant difference compared with *PHLDA3*$^{+/+}$ islets, indicating that *PHLDA3*$^{-/-}$ islets retain normal β cell characteristics, to the extent we examined.

***PHLDA3*-Deficient Islets Have Enhanced Akt Activity and Larger Cell Size, and Are Resistant to Apoptosis.** We further analyzed the effects of PHLDA3 deficiency on several Akt-regulated biological processes. We first confirmed reduction or loss of *PHLDA3* expression in *PHLDA3*$^{+/-}$ and *PHLDA3*$^{-/-}$ mice islets (Fig. 8*A*). We found that activation of Akt and phosphorylation of its downstream molecules were augmented in *PHLDA3*$^{-/-}$ islets (Fig. 8*B*). It has been reported that enhanced Akt activity has an effect on islet cell size (5, 6). We therefore analyzed islet cell size in *PHLDA3*$^{+/+}$, *PHLDA3*$^{+/-}$, and *PHLDA3*$^{-/-}$ mice. As shown in Fig. 8*C*, islet cell size was significantly increased in *PHLDA3*$^{-/-}$ and *PHLDA3*$^{+/-}$ mice. We next analyzed the sensitivity of *PHLDA3*$^{-/-}$ islets to apoptosis. Wild-type or *PHLDA3*$^{-/-}$ mice were treated with STZ for 5 consecutive days to produce β cell injury. It is known that STZ-induced apoptosis of β

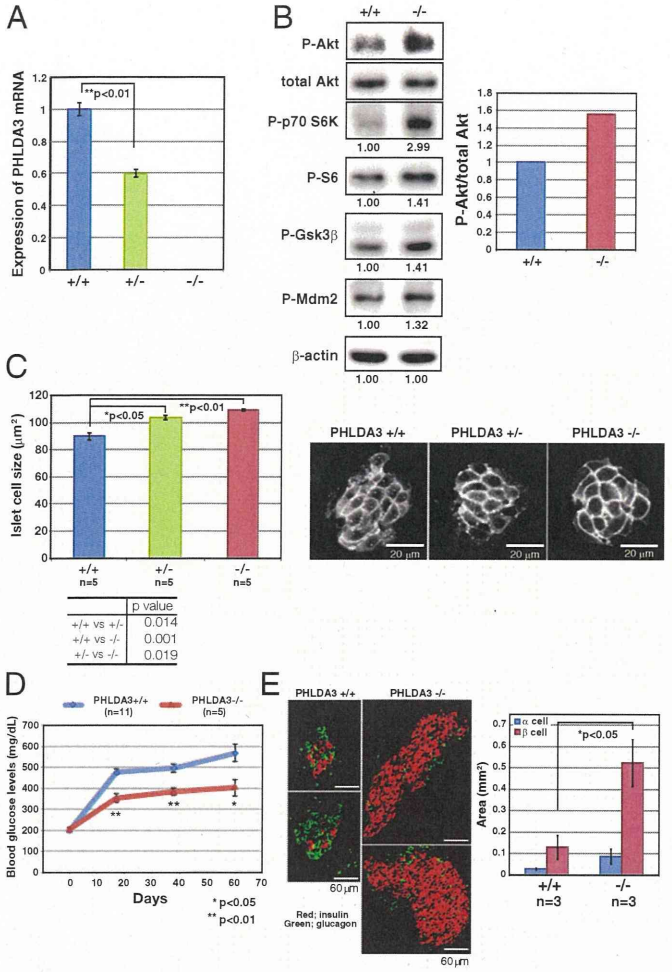

Fig. 8. Akt activation in islets of *PHLDA3*-deficient mice. (*A*) *PHLDA3* mRNA expression in isolated islets. Islets were isolated from $PHLDA3^{+/+}$, $PHLDA3^{+/-}$, and $PHLDA3^{-/-}$ mice, and analyzed for *PHLDA3* expression by quantitative RT-PCR, normalized to β-actin. (*B*) Akt activity and phosphorylation of Akt downstream signaling molecules in isolated islets. Akt activation and phosphorylation of Akt downstream signaling molecules were analyzed by Western blotting and quantified by normalization to total Akt levels (P-Akt, *Right*) or by β-actin levels (P-p70 S6K, P-S6, P-GSK3β, and P-Mdm2). (*C*) Islet cell size in *PHLDA3*-deficient mice. (*Left*) Indirect immunofluorescence staining of Glut2 in pancreas section from 10-mo-old mice. (*Right*) Islet areas and nuclei numbers were calculated, and mean islet cell sizes were determined from one hematoxylin- and eosin-stained pancreas sections per indicated numbers (n) of mice. The *P* values between $PHLDA3^{+/+}$ and $PHLDA3^{+/-}$ or $PHLDA3^{-/-}$ were calculated and shown in the panels (*$P < 0.05$; **$P < 0.01$). The difference between $PHLDA3^{+/-}$ and $PHLDA3^{-/-}$ was also significant ($P < 0.05$). (*D*) Blood glucose levels in streptozotocin-induced diabetic mice. Indicated numbers (n) of $PHLDA3^{+/+}$ or $PHLDA3^{-/-}$ mice were injected i.p. with STZ for 5 consecutive days. Blood glucose levels were determined at different time points as indicated after administration of STZ. (*$P < 0.05$; **$P < 0.01$). (*E*) Distribution of β and α cells in STZ-treated $PHLDA3^{+/+}$ and $PHLDA3^{-/-}$ mice. (*Left*) Sections were stained with antibody against insulin (β cell marker; red) and glucagon (α cell marker; green) and representative images are shown. Pancreas sections of three $PHLDA3^{+/+}$ and three $PHLDA3^{-/-}$ mice were analyzed. (*Right*) For each mouse, α-cell and β-cell areas were calculated from one pancreas section. (*$P < 0.05$.)

cell results in the elevation of blood glucose, and can thereby experimentally induce type I diabetes in mice. We analyzed blood glucose levels at the indicated times following STZ treatment, and STZ administration resulted in the effective elevation of blood glucose levels in wild-type mice, whereas elevation was diminished in $PHLDA3^{-/-}$ mice (Fig. 8*D*). When we calculated β cell and α cell areas in STZ-treated mice, we observed a significant increase in the area occupied by β cells in *PHLDA3*-deficient mice, showing that PHLDA3 is required for the efficient induction of β cell apoptosis by STZ (Fig. 8*E*). These results demonstrate that PHLDA3 controls Akt activity, cell size, and apoptosis of islet cells in vivo.

Discussion

In this report, we have shown that PHLDA3 is a candidate tumor suppressor in PanNETs. We observed that the LOH of the *PHLDA3* gene locus in human PanNETs occurs at a remarkably high frequency and is comparable to that of the *MEN1* gene locus, the gene reported to be most frequently affected in PanNETs (15). We also showed that LOH at the *PHLDA3* gene locus is associated with disease progression and poor prognosis in PanNETs. In contrast, LOH/mutation of *MEN1* was found to be unrelated to the prognosis of PanNET patients, both in this and in a previous study (7). These results show that the PHLDA3-regulated tumor suppression pathway is relevant to the progression and malignant phenotype of PanNETs and the poor prognosis of PanNET patients. Because PHLDA3 is a repressor of Akt, we propose that inhibition of the Akt pathway would improve the prognosis of PanNET patients exhibiting LOH of *PHLDA3*. This possibility is supported by the reported clinical efficacy of the Akt pathway inhibitor Everolimus, which has been shown to improve the survival of PanNET patients significantly. Everolimus treatment was approved in Japan only from 2011, and therefore none of the patients in our study had received Everolimus. We speculate that patients who are positive for *PHLDA3* LOH and have a poor prognosis may benefit most from Everolimus treatment. Furthermore, determination of *PHLDA3* LOH status could serve as a diagnostic measure to select patients who should receive Everolimus. Thus, it will be important to conduct a prospective study to analyze the effect of Everolimus in patients with or without *PHLDA3* LOH.

We have shown that PHLDA3 regulates Akt activity and various Akt-regulated biological processes, i.e., cell proliferation, cell size, and apoptosis, in cultured cell lines and in vivo endocrine cells. Several laboratories have generated transgenic mice that specifically express active Akt in β cells (6, 16). These mice developed hyperplastic islets, but did not develop malignant PanNETs (17). Likewise, we have shown that loss of PHLDA3 and the resulting activation of Akt leads to hyperplastic islet development, but not to the development of PanNETs. Although Akt activation is observed in various cancers and contributes to tumorigenesis and tumor progression, the conclusion derived from these experiments is that activation of Akt pathway alone is insufficient to cause PanNETs unless combined with an oncogenic event in a second pathway. In human PanNETs, double LOH of *PHLDA3* and *MEN1* is frequently observed. In these cells, loss of PHLDA3 function, i.e., activation of Akt, is combined with loss of MEN1 function to promote PanNET tumorigenesis, and loss of PHLDA3 function particularly contributes to the progression of PanNETs. It would therefore be interesting to generate mice that are doubly deficient in *PHLDA3* and *MEN1* to analyze whether the islet phenotypes are more pronounced and the hyperplastic islets more prone to malignancy.

We observed hyperplastic islets in *PHLDA3* heterozygote (+/−) mice as well as *PHLDA3*-deficient (−/−) mice. This observation suggests that *PHLDA3* is haplo-insufficient for the suppression of endocrine cell proliferation. We have previously shown that PHLDA3 expression represses Akt activity in a dose-dependent manner, consistent with the possibility that loss of a single *PHLDA3* allele could lead to enhanced Akt activation and enhanced proliferation of endocrine cells (8). However, we have also shown that in human PanNETs, the *PHLDA3* locus undergoes methylation in addition to LOH, suggesting that two hits on the *PHLDA3* gene is required for human PanNET development. We assume that loss of both *PHLDA3* alleles, and consequent stronger activation of Akt, may be required to exert a tumorigenic phenotype. Future studies should examine the islet phenotypes of $PHLDA3^{+/-}$ and $PHLDA3^{-/-}$ in a $MEN1^{-/-}$ back-

ground. We expect that, in a *MEN1*$^{-/-}$ background, *PHLDA3*$^{-/-}$ mice would develop PanNETs more frequently than in *PHLDA3*$^{+/-}$ mice. In addition, because we found association of LOH at the *PHLDA3* locus in both nonfunctional and functional human PanNETs, whether nonfunctional PanNETs develop in these mice is an interesting issue.

We previously identified *PHLDA3* as a p53 target gene. In the present study, we show that the *PHLDA3* locus undergoes frequent LOH in PanNETs, a tumor type in which p53 mutations are rare (3, 7). Recently it has been reported that among the various target genes of p53, *PHLDA3* displays prominent tumor suppressor activity (18). Therefore, in tumors harboring a p53 mutation, loss of p53-regulated *PHLDA3* expression may significantly contribute to tumor progression, whereas in tumors without a p53 mutation, loss of the *PHLDA3* gene itself may drive oncogenesis. Interestingly, global methylation profiling of prostate cancer specimens has revealed significant methylation of the *PHLDA3* gene in these cancers (19). In addition, in the COSMIC database, 11 PHLDA3 mutations in several cancers are reported. All mutations are located within the PH domain of PHLDA3, and nonsynonymous mutations may result in loss of Akt repressing ability. Therefore, in addition to inactivation by methylation, these and other mutations that result in a functional loss of PHLDA3 may contribute to some cancers.

In summary, our results show that PHLDA3 is a novel tumor suppressor of PanNET, and PHLDA3 and MEN1 cooperatively suppress its development. PHLDA3 represses Akt activity in islet cells and hyperplastic islets are found in both *PHLDA3*$^{+/-}$ and *PHLDA3*$^{-/-}$ mice. Collectively, our data illustrates the importance of the PHLDA3-regulated tumor suppression pathway in PanNETs.

Materials and Methods

Cell Lines, Cell Culture, Transfection, Adenovirus Infection, and Soft Agar Colony Formation Assay. Cell lines used in this study were: LNCaP (human prostate cancer), MDA-MB-M468 (human breast cancer), DLD1 (human colorectal cancer), H1299 (human lung NET), A99 (human PanNET, ref. 20), RIN (rat pancreatic β cell), and MIN6 (mouse pancreatic β cell). Cell culture and transfection was performed as described (21). The siRNAs were introduced using RNAiMAX (Invitrogen). ON-target plus control and ON-target plus PHLDA3-targeting siRNAs were purchased from Dharmacon Research. Adenovirus infection was performed using previously described adenoviruses expressing LacZ or N-terminally HA-tagged PHLDA3 (8). Everolimus (AdooQ BioScience) was added to cultures at the indicated concentrations. For soft agar colony formation assays, cells were seeded in 3-cm dishes with a bottom layer of 0.5% agarose and a top layer of 0.33% agarose, both in complete media. The assay was performed in triplicate for each sample. Colonies were photographed after 9 (H1299) or 10 (MIN6) days of incubation. Colonies were counted in three to five different views from each plate to calculate average values. The total numbers of colonies larger than 100 (MIN6) or 200 (H1299) pixels were counted per view.

Western Blotting Analysis. Cells were lysed in lysis buffer [50 mM Tris·HCl (pH 8.0), 1% Nonidet P-40, 250 mM NaCl, 50 mM NaF, 1 mM Na_3VO_4, 1 mM protease inhibitor (PMSF, aprotinin, leupeptin) and 1 mM DDT]. Whole cell lysates were subjected to protein quantification and analyzed by Western blotting. To detect PHLDA3, 20 μg of whole cell lysates (WCL) were loaded. To detect other proteins, 5 μg of WCL were loaded. Antibodies used in this study were: anti-Akt rabbit polyclonal antibody, anti-phospho-Akt (S473) rabbit monoclonal antibody, anti-p70S6K rabbit monoclonal antibody, anti-phospho-p70S6K (T389) rabbit polyclonal antibody, anti-phospho-S6 (S240/244) rabbit monoclonal antibody, anti-phospho-Gsk3β (S9) rabbit polyclonal antibody, anti-phospho-Mdm2 (S166) rabbit polyclonal antibody from Cell Signaling Technology, anti-actin mouse monoclonal antibody from SIGMA from Santa Cruz Biotechnology, anti-PHLDA3 goat polyclonal antibody from Abcam, anti-HA monoclonal antibody (clone 12CA) from Roche Diagnostics.

Reverse Transcription and Real-Time PCR. Reverse transcription was carried out using kits from Invitrogen following the manufacturer's instructions (SuperScript First-Strand Synthesis System for RT-PCR). Total RNA (0.2–5 μg) was used for reverse transcription. Reverse-transcribed cDNAs were subjected to real-time PCR, which was performed with a LightCycler 480 Instrument (Roche Diagnostics). For the detection of PHLDA3 (human; Hs00385313_m1, mouse; Mm00449846_m1, rat; rat; Rn01483684_m1), beta actin (mouse; Mm00607939_s1, rat; Rn00667869_m1) and GAPDH (human; Hs02758991_g1, mouse; Mm99999915_g1), TaqMan probe from Applied Biosystems was used.

BrdU Incorporation Assay and Measurement of Cell Number. BrdU-positive cells were quantified using the Ziva Ultrasensitive BrdU assay (Jaden BioScience). This assay detects the incorporation of BrdU using a labeled anti-BrdU antibody and detection substrate in an ELISA format. By this assay, a small fraction of proliferating cells within a large population of nonproliferating cells can be detected. Cell numbers were analyzed by using CellTiter-Glo Luminescent Cell Viability Assay (Promega). Using this assay, viable cells are determined by quantitation of ATP, an indicator of metabolically active cells.

Flow Cytometry and TUNEL Assay. Apoptosis of islet cells was quantitated by the TUNEL reaction using the In Situ Cell Death Detection kit, Fluorescein (Roche Diagnostics) followed by flow cytometry. Flow cytometry analysis was performed using a FACS Calibur instrument (Becton Dickinson).

Tumor Samples Used in the Study, and DNA and RNA Extraction from Primary Tumor Samples. The tumor samples used in this study were surgically resected at the National Cancer Center Hospital (44 samples; PanNET1-18, 24–47, 52, 53), Kyoto University Hospital (6 samples; PanNET19-23, 51), or Kagawa University Hospital (4 samples; PanNET 48–50, 54) between 1993 and 2012. Histological grading of the tumors were determined based on the classification of World Health Organization 2004. This study was approved by the Institutional Review Board of the National Cancer Center, Tokyo. Clinical and pathological data were obtained through a detailed retrospective review of the medical records of all patients with PanNET. Five-micrometer sections of paraffin-embedded tissues were subjected to DNA extraction. Total RNA was extracted from frozen normal pancreas and tumor samples using an RNeasy mini kit (Qiagen).

Microsatellite Analysis. Microsatellite analysis was performed basically as described (8). We used six primer pairs labeled with FAM that amplify microsatellite loci to achieve accurate detection of LOH at the *PHLDA3* locus (Fig. 1*A*). For the *MEN1* locus, three primer pairs were used (Fig. 2*A*). Amplified PCR products were analyzed with a 3100 automated sequencer (Applied Biosystems). Collected data were analyzed with GeneScan and Genotyper software (Applied Biosystems), and allele sizes and peak heights were calculated. The genotype was determined to be heterozygous if two bands of different sizes were obtained from normal tissues. A ratio of the two peaks in tumor DNA of less than 0.7 in comparison with the corresponding ratio of the two peaks in nontumor DNA was considered as allelic loss.

5-aza-dC Treatment and Methylation-Specific PCR. Cells were seeded at a density of 3×10^5 cells (H1299 and A99) or 3×10^6 (MIN6) cells per 10-cm dish on day 0 and treated with freshly prepared 5-aza-dC (Sigma-Aldrich) for 24 h on days 1, 3, and 5. After each treatment, cells were placed in fresh medium and harvested on day 6. Genomic DNA was extracted and subjected to bisulfite conversion using EZ DNA Methylation kit (Zymo research). Fully methylated controls were prepared by methylating genomic DNA with SssI methylase (New England Biolabs). Methylation-specific PCR (MSP) was performed basically as described (22). MSP was performed using the specific primer sets shown below. BS-F and R primers were used to amplify DNA with or without methylation. MSP-F and R primers were used to amplify methylated DNA.

BS-F: GTAGATAGAGTTTAGGGGAGTAAGAG

BS- R: CTCTACCCCAACTAACCCAACCC

MSP-F: GAGGGTTGGTTAGGGTAGGAATGTG

MSP-R: ACTCCCCTAAACTCTATCTACACAC

Mice Used in This Study. Generation of *PHLDA3*-deficient mice was reported (23). Briefly, a *PHLDA3*neo targeting vector was obtained by cloning a 6-kb upstream KpnI fragment and a 6-kb downstream HindIII/NotI fragment into pPNT1. The resulting deletion (nucleotides 579–2,096 of GenBank accession no. AF151099) eliminates all of exon 1 and part of exon 2, thus deleting the entire *PHLDA3* coding region. *PHLDA3*$^{-/-}$ mice were generated by crossing the heterozygotes. MEFs were isolated and maintained as described (24). Mouse experiments were performed in a specific pathogen-free environment at the National Cancer Center animal facility according to institutional guidelines, and all of the animal experiments were approved by the Committee for Ethics in Animal Experimentation at the National Cancer Center.

Blood Glucose, Plasma Insulin Measurement, and Glucose Tolerance Tests. Blood glucose levels were determined with blood samples from tail vein

punctures in mice using Glucose pilot (Aventir Biotech), according to the procedures specified by the manufacturer. Plasma insulin levels were determined with blood samples from tail vein punctures or inferior vena cava in mice by ELISA (Morinaga Institute of Biological Science), according to the procedures specified by the manufacturer. For glucose tolerance tests, mice were fasted overnight and blood was drawn from tail vein at 0, 15, 30, 45, 60, 90, and 120 min after i.p. injection of D-glucose (2 mg/g of body weight).

Quantitative Measurement of Islet Morphology. Islet area and islet nuclei number were measured from hematoxylin and eosin-stained pancreas sections and Ki67-positive cells were counted from immunohistochemically stained pancreas sections using TissueFAXS (TissueGnostics). Chromogranin A signal intensity was also measured using TissueFAXS. α and β cells areas were quantified by the number of pixels in each immunohistochemically stained area in images taken by fluorescence microscopy (Olympus IX2-DSU).

Isolation of Rat and Mouse Primary Islets and Preparation of Primary Islet Cells. The animal experiment was reviewed and approved by the Institutional Animal Care and Use Committee for Frontier Medical Sciences, Kyoto University. For isolation of rat islets, Lewis or Wistar rats (male, aged 9–11 wk, Shimizu Laboratory Supplies) were used. Islet isolation was performed according to previously described methods (25). Briefly, through midline laparotomy, 10 mL of a type XI collagenase solution (1200 CDU/mL, C9407, Sigma-Aldrich) was infused into the common bile duct that was ligated at the hepatic side before the inflow into the duodenum. The pancreases were removed and digested in a water bath set at 37 °C for 18 min. The digested pancreases were filtered with a stainless steel sieve to separate the islets, and purified using a discontinuous gradient solution (Dextran 70, 17–0280-02, Amersham). Mouse islets were isolated from 10- to 25-wk-old male animals by collagenase digestion of the pancreas, followed by purification using a Ficoll gradient. Islets were handpicked twice. The harvested islets were cultured in RPMI or CRML-1066 medium (11530, Gibco) supplemented with a 1% antibiotic–antimycotic solution (15240-062, Gibco) and 10% (vol/vol) FBS (12103-78P, JRH) in an incubator set at 5% (vol/vol) CO_2, 37 °C.

Primary islet cells were prepared by digesting the islets with Accutase for 15 min at 37 °C. Islet cells were washed with RPMI before use in experiments.

Immunohistochemistry. Immunohistochemistry (IHC) was performed basically according to the manufacturer's instructions. In brief, after deparaffinization, tissues sections underwent antigen retrieval by autoclaving slides for 5 min in 10 mM citrate buffer (pH 6.0). For fluorescent immunohistochemical staining of insulin, glucagon, and Glut2, nonspecific interactions were blocked for 30 min using a 5% (vol/vol) goat serum solution. The primary antibodies were: guinea pig anti-insulin polyclonal antibody (Abcam) diluted 1:400, mouse anti-glucagon monoclonal antibody (Sigma-Aldrich) diluted 1:750 and rabbit anti-Glut2 polyclonal antibody (Alpha Diagnostic) diluted 1:750 with Signal Enhancer HIKARI (Nacalai Tesque). These were applied to the slides and incubated overnight at 4 °C. As secondary antibodies, Alexa Fluor 488 goat anti-mouse IgG antibody (Invitrogen) diluted 1:500, Alexa Fluor 488 goat anti-rabbit IgG antibody (Invitrogen) diluted 1:500 and Alexa Fluor 546 goat anti-guinea pig IgG antibody (Invitrogen) diluted 1:1,000 with PBST-BSA were applied to the slides and incubated 3 h at room temperature. To detect Ki67- and Chromogranin A-positive cells, sections were pretreated with 0.3% H_2O_2 for inactivation of endogenous peroxidase. The primary antibody, rat anti-Ki67 monoclonal antibody (DakoCytomation) diluted 1:200, or rabbit anti-Chromogranin A polyclonal antibody (Thermo Scientific) diluted 1:200 with Signal Enhancer HIKARI were applied to the slides and incubated overnight at 4 °C. As secondary antibodies, Histofine Simple Stain MAX PO anti-rat IgG antibody (Nichirei Bioscience) or biotinylated anti-rabbit IgG antibody (VECTOR Laboratories) was used. We used 3,3′-diaminobenzidine tetrahydrochloride (DAB; Muto Pure Chemicals) as the substrate chromogen. The sections were counter stained with hematoxylin.

STZ-Induced Diabetes. Eleven- to 22-wk-old wild-type and *PHLDA3* knockout male mice were injected i.p. with 50 mg/kg streptozotocin daily for 5 consecutive days (Sigma-Aldrich) to produce β cell injury. On days 92, 93, 99, and 100, animals were killed.

Statistical Analysis. Data were calculated and shown as mean ± SD (for Figs. 4, 5 and *SI Appendix*, Fig. S3) or as mean ± SEM (Figs. 6–8 and *SI Appendix*, Figs. S7, S9, and S10*A*). Comparisons between the samples were performed by Student *t* test. Survival data were analyzed using XLStat software (version 2013.4.05; Addinsoft), and Kaplan–Meyer plots were drawn. Wilcoxon test was performed to assess the statistical significance of the difference between the survival curves. In Fisher's exact test, *P* values were obtained by using two tails. Statistical significance was defined as $P < 0.05$.

ACKNOWLEDGMENTS. We thank T. Niwa and T. Ushijima (National Cancer Center, Japan) for advice on methylation-specific PCR, Marc Lamphier for critical reading of the manuscript, Dr. Wanxing Cui for providing isolated human islets, and Drs. T. Yoshida and H. Sakamoto and National Cancer Center Research Core Facility (supported by National Cancer Center Research and Development Fund, 23-A-7) for the LOH analyses in this study. This study was supported by Grants-in-Aid for Scientific Research from the Ministry of Education, Culture, Sports, Science and Technology of Japan (23501279 and 26430133, to R.O.); New Energy and Industrial Technology Development Organization (NEDO) (09A02012a, to R.O.); research grants from Daiichi-Sankyo Foundation of Life Science (to R.O.); the Ichiro Kanehara Foundation (R.O.); Takeda Science Foundation (R.O.); Astellas Foundation for Research on Metabolic Disorders (R.O.); Foundation for Promotion of Cancer Research in Japan (R.O.); Extramural Collaborative Research Grant of Cancer Research Institute, Kanazawa University, Japan (to R.O.); Cooperative Research Program of Institute for Frontier Medical Sciences, Kyoto University, Japan (R.O.); and grants from the National Cancer Center Research and Development Fund (23-B-9, to R.O.; and 23-A-11, to T.T.).

1. Hauso O, et al. (2008) Neuroendocrine tumor epidemiology: Contrasting Norway and North America. *Cancer* 113(10):2655–2664.
2. Yao JC, et al. (2008) One hundred years after "carcinoid": Epidemiology of and prognostic factors for neuroendocrine tumors in 35,825 cases in the United States. *J Clin Oncol* 26(18):3063–3072.
3. de Wilde RF, Edil BH, Hruban RH, Maitra A (2012) Well-differentiated pancreatic neuroendocrine tumors: From genetics to therapy. *Nat Rev Gastroenterol Hepatol* 9(4):199–208.
4. Yao JC, et al.; RAD001 in Advanced Neuroendocrine Tumors, Third Trial (RADIANT-3) Study Group (2011) Everolimus for advanced pancreatic neuroendocrine tumors. *N Engl J Med* 364(6):514–523.
5. Elghazi L, Bernal-Mizrachi E (2009) Akt and PTEN: Beta-cell mass and pancreas plasticity. *Trends Endocrinol Metab* 20(5):243–251.
6. Tuttle RL, et al. (2001) Regulation of pancreatic beta-cell growth and survival by the serine/threonine protein kinase Akt1/PKBalpha. *Nat Med* 7(10):1133–1137.
7. Jiao Y, et al. (2011) DAXX/ATRX, MEN1, and mTOR pathway genes are frequently altered in pancreatic neuroendocrine tumors. *Science* 331(6021):1199–1203.
8. Kawase T, et al. (2009) PH domain-only protein PHLDA3 is a p53-regulated repressor of Akt. *Cell* 136(3):535–550.
9. Yang YM, et al. (2005) Chromosome 1q loss of heterozygosity frequently occurs in sporadic insulinomas and is associated with tumor malignancy. *Int J Cancer* 117(2):234–240.
10. Chen YJ, Vortmeyer A, Zhuang Z, Huang S, Jensen RT (2003) Loss of heterozygosity of chromosome 1q in gastrinomas: Occurrence and prognostic significance. *Cancer Res* 63(4):817–823.
11. Corbo V, et al. (2010) MEN1 in pancreatic endocrine tumors: Analysis of gene and protein status in 169 sporadic neoplasms reveals alterations in the vast majority of cases. *Endocr Relat Cancer* 17(3):771–783.
12. Yoo NJ, Kim YR, Lee SH (2011) Expressional and mutational analysis of PHLDA3 gene in common human cancers. *Pathology* 43(5):510–511.
13. Brenet F, et al. (2011) DNA methylation of the first exon is tightly linked to transcriptional silencing. *PLoS ONE* 6(1):e14524.
14. Lenzen S (2008) The mechanisms of alloxan- and streptozotocin-induced diabetes. *Diabetologia* 51(2):216–226.
15. Pannett AA, Thakker RV (1999) Multiple endocrine neoplasia type 1. *Endocr Relat Cancer* 6(4):449–473.
16. Bernal-Mizrachi E, Wen W, Stahlhut S, Welling CM, Permutt MA (2001) Islet beta cell expression of constitutively active Akt1/PKB alpha induces striking hypertrophy, hyperplasia, and hyperinsulinemia. *J Clin Invest* 108(11):1631–1638.
17. Vivanco I, Sawyers CL (2002) The phosphatidylinositol 3-Kinase AKT pathway in human cancer. *Nat Rev Cancer* 2(7):489–501.
18. Brady CA, et al. (2011) Distinct p53 transcriptional programs dictate acute DNA-damage responses and tumor suppression. *Cell* 145(4):571–583.
19. Mahapatra S, et al. (2012) Global methylation profiling for risk prediction of prostate cancer. *Clin Cancer Res* 18(10):2882–2895.
20. Yachida S, et al. (2011) Establishment and characterization of a new cell line, A99, from a primary small cell carcinoma of the pancreas. *Pancreas* 40(6):905–910.
21. Ozeki C, et al. (2011) Cancer susceptibility polymorphism of p53 at codon 72 affects phosphorylation and degradation of p53 protein. *J Biol Chem* 286(20):18251–18260.
22. Yamashita S, Tsujino Y, Moriguchi K, Tatematsu M, Ushijima T (2006) Chemical genomic screening for methylation-silenced genes in gastric cancer cell lines using 5-aza-2′-deoxycytidine treatment and oligonucleotide microarray. *Cancer Sci* 97(1):64–71.
23. Frank D, et al. (2002) Placental overgrowth in mice lacking the imprinted gene Ipl. *Proc Natl Acad Sci USA* 99(11):7490–7495.
24. Ohki R, et al. (2000) Reprimo, a new candidate mediator of the p53-mediated cell cycle arrest at the G2 phase. *J Biol Chem* 275(30):22627–22630.
25. Yang KC, et al. (2010) The cytoprotection of chitosan based hydrogels in xenogeneic islet transplantation: An in vivo study in streptozotocin-induced diabetic mouse. *Biochem Biophys Res Commun* 393(4):818–823.

Germline deletion and a somatic mutation of the *PRKAR1A* gene in a Carney complex-related pituitary adenoma

T Iwata*, T Tamanaha*[1,*], R Koezuka[1], M Tochiya[1], H Makino[1], I Kishimoto[1], N Mizusawa, S Ono, N Inoshita[2], S Yamada[3], A Shimatsu[4] and K Yoshimoto

Department of Medical Pharmacology, Institute of Health Biosciences, The University of Tokushima Graduate School, Kuramoto-cho 3-18-15, Tokushima 770-8504, Japan, [1]Department of Endocrinology and Metabolism, National Cerebral and Cardiovascular Center, Osaka, Japan, Departments of [2]Pathology and [3]Hypothalamic and Pituitary Surgery, Toranomon Hospital, Tokyo, Japan and [4]Clinical Research Institute, National Hospital Organization Kyoto Medical Center, Kyoto, Japan
*(T Iwata and T Tamanaha contributed equally to this work)

Correspondence should be addressed to K Yoshimoto
Email
yoshimoto@tokushima-u.ac.jp

Abstract

Objective: The objective was to assess involvement of loss of the *PRKAR1A* gene encoding a type 1α regulatory subunit of cAMP-dependent protein kinase A located on 17q24 in a Carney complex (CNC)-related pituitary adenoma.
Design: We investigated aberrations of the *PRKAR1A* gene in a CNC patient with a GH-producing pituitary adenoma, whose family has three other members with probable CNC.
Methods: A gene mutation was identified by a standard DNA sequencing method based on PCR. DNA copy number was measured to evaluate allelic loss on 17q24 by quantitative PCR. The breakpoints of deletion were determined by cloning a rearranged region in the deleted allele.
Results: A *PRKAR1A* mutation of c.751_758del8 (p.S251LfsX16) was found in genomic DNA obtained from a pituitary adenoma, but not leukocytes from the patient. Reduced DNA copy number at loci including the *PRKAR1A* gene on 17q24 was detected in both the tumor and leukocytes, suggesting a deletion at the loci at the germline level. The deletion size was determined to be ~0.5 Mb and this large deletion was also found in two other family members.
Conclusion: This is the first case showing a CNC-related pituitary adenoma with the combination of somatic mutation and a large inherited deletion of the *PRKAR1A* gene. Biallelic inactivation of *PRKAR1A* appears to be necessary for the development of CNC-related pituitary adenoma.

European Journal of Endocrinology (2015) **172**, K5–K10

European Journal of Endocrinology

Introduction

The complex of 'spotty-skin pigmentation, myxomas, endocrine overactivity, and schwannomas' or Carney complex (CNC) (MIM 160980) is an autosomal dominant multiple neoplasia syndrome (1). CNC is an inherited predisposition to tumors associated with primary pigmented nodular adrenocortical disease (PPNAD), GH- and/or PRL-producing pituitary adenoma, myxomas of heart or skin, psammomatous melanotic schwannoma, and breast ductal adenoma (2).

Previous studies have shown inactivating germline mutations in the *PRKAR1A* gene on 17q24, which may function as a tumor-suppressor gene, in patients with CNC (3, 4). The encoded protein is a type 1α regulatory subunit of cAMP-dependent protein kinase A (PKA). Inactivating germline mutations of this gene are found in ~70% of patients with CNC (2, 5). Salpea *et al.* (6) have recently reported that 17q24.2–24.3 deletions of varying size including the *PRKAR1A* gene led to haploinsufficiency

www.eje-online.org
DOI: 10.1530/EJE-14-0685

Published by Bioscientifica Ltd.

in 11 CNC patients without *PRKAR1A* mutations. Less commonly, the molecular pathogenesis of CNC is a variety of genetic changes on 2p16 (7).

Previous studies have shown that biallelic inactivation of *PRKAR1A* is needed for tumor development in the adrenal and other tissues (8, 9). In addition, biallelic, but not monoallelic, inactivation of *Prkar1a* in mouse pituitary gland leads to the development of a pituitary tumor (10) and several pituitary tumors in CNC patients have been shown to have bilallelic abnormalities of *PRKAR1A* (4, 11, 12). In this study, we examined the *PRKAR1A* locus in a Japanese family with CNC and found a large germline deletion of the locus and biallelic inactivation of *PRKAR1A* in a pituitary adenoma.

Subjects and methods

Case report

The proband was a young woman who presented with pituitary gigantism and pigmented spots on the face and lips. She had been tall during her childhood and reached a height of 183.5 cm. Incidental pituitary adenoma with a diameter of 15 mm was revealed by magnetic resonance imaging (MRI) upon investigating her head injury (Fig. 1A). She had increased serum levels of GH (11.0 μg/l) and IGF1 (590 μg/l), and the GH levels were not suppressed during oral glucose tolerance test. Serum levels of PRL and cortisol were within the normal range. She had undergone successful endoscopic transnasal adenomectomy at Toranomon Hospital, and the resected pituitary adenoma showed an unusual unique histological feature. The adenoma was composed of extremely enlarged eosinophilic cells harboring large nuclei with prominent nucleoli (Fig. 1B). Immunohistochemical study revealed that tumor cells were positive to an anti-GH antibody (A0570; Dako, Glostrup, Denmark) and negative to an antibody against type 1α regulatory subunit of PKA (#610610; BD Biosciences, San Jose, CA, USA) compared with adjacent normal cells (Fig. 1C and D).

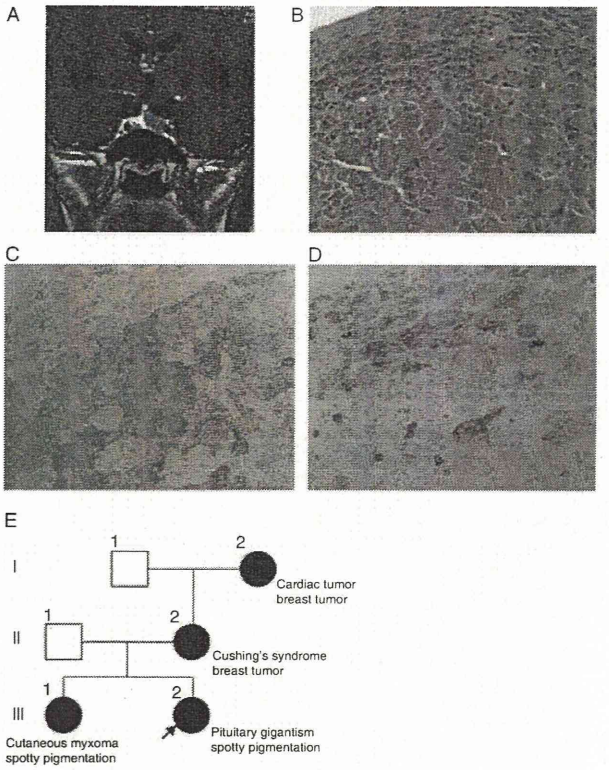

Figure 1

Preoperative coronal T1-weighted enhanced MRI of the proband and histopathology of a pituitary tumor. (A) MRI demonstrates a pituitary tumor (15 mm in diameter) located in the left wing. (B, C, and D) Hematoxylin and eosin staining (B) and immunostaining using antibodies against GH (C) and type 1α regulatory subunit of PKA (D) in serial sections of pituitary adenoma with adjacent normal pituitary cells (left upper side). (E) A pedigree of the CNC family and histological findings of tumors. The proband is indicated by an arrow. Family members are indicated by generation (roman numerals) and individuals (arabic numerals). Individuals are represented as male (squares) and female (circles). Filled symbols denote patients with CNC. A full colour version of this figure is available via http://dx.doi.org/10.1530/EJE-14-0685.

Family history

Her family history was remarkable; her mother (II-2 in Fig. 1E) had been operated on for a right adrenal tumor due to Cushing's syndrome at the age of 19 and her grandmother (I-2) for a cardiac tumor at the age of 48. Both mother and grandmother had been operated on for breast tumors, at ages of 52 and 68 respectively. An elder sister (III-1) underwent surgical operations for a gingival tumor at the age of two and eyelid tumors at ages of 13 and 16. One of the eyelid tumors was pathologically diagnosed as cutaneous myxoma. Spotty facial pigmentation was present.

This study was approved by ethics committees of Toranomon Hospital and the University of Tokushima. Individual informed consents for genomic analyses and case presentations were obtained from patients.

Gene mutation analysis

Gene mutation analysis for the *PRKAR1A* gene using PCR and sequencing was performed as described previously (13). Genomic DNA isolated from leukocytes and a frozen pituitary adenoma was subjected to PCR using TaKaRa Ex Taq Polymerase (TaKaRa, Shiga, Japan) with the *PRKAR1A* primer sets. PCR products were subjected to direct sequencing in sense and antisense directions.

DNA copy number analysis in a tumor and leukocytes

Relative DNA copy number at each locus on 17q24 was measured by quantitative PCR (qPCR) in a 7300 Real Time PCR System (Applied Biosystems) using THUNDERBIRD SYBR qPCR mix (Toyobo, Osaka, Japan) with each primer set shown in Supplementary Table, see section on supplementary data given at the end of this article. The specificity of the primer pairs was verified by dissociation curves and the quantitativity was confirmed by slopes in the standard samples for the target loci being between −3.6 and −3.2 and each R2 value being between 0.99 and 1. The DNA copy number was normalized using that of human TATA-binding protein (*TBP*) located on 6q27. Furthermore, DNA copy numbers of albumin (*ALB*) on 4q13.3 or telomerase reverse transcriptase (*TERT*) on 5p15.33 were confirmed to be almost equal among the samples.

Detection of deleted allele on 17q24 in the subjects

DNA encompassing the deletion junction on 17q24 was amplified from each subject's leukocyte genomic DNA using TaKaRa Ex Taq Polymerase with the following primers: forward: 5′-GGGACCATCCTGGCTAACACG-3′ and reverse: 5′-GGACATCTGACCTACAAAACTGTGAGC-3′. Normal female DNA (Promega) and pBluescript II SK+ with a DNA fragment including the deletion junction were used as a negative control and a positive control, respectively. PCR using a primer set for the *TERT* gene as an internal control was also carried out.

Results

Somatic mutation and one-copy deletion of the *PRKAR1A* gene in a pituitary adenoma

We examined mutations of the *PRKAR1A* gene in genomic DNA from a pituitary adenoma and from leukocytes of a proband (III-2 in Fig. 1E) and her parents (II-1 and II-2), using direct sequencing of 11 overlapping PCR products with primer sets that cover the entire coding region and splicing junctions. Sequencing analysis showed no mutations in the *PRKAR1A* gene in leukocyte genomic DNA from all subjects, but a somatic mutation of c.751_758del8 (p.S251LfsX16) in exon 8 of the *PRKAR1A* gene in a pituitary adenoma (Fig. 2A). Intensities of WT sequence peaks were weaker than those of mutated allele in the tumor sample, suggesting that these sequence peaks might be derived from the normal allele of slightly contaminated normal tissue and the other allele might be lost at the germline level. To demonstrate the deletion at 17q24, DNA copy number of the *PRKAR1A* gene was measured by qPCR using five primer sets as shown in Fig. 2B (upper diagram). The DNA copy numbers of the *PRKAR1A* gene were reduced by almost half in leukocyte

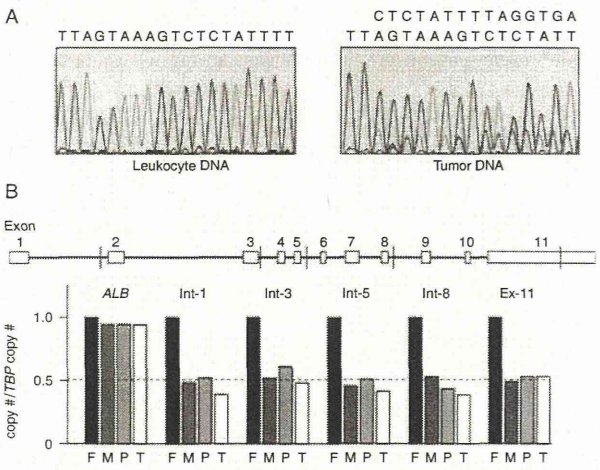

Figure 2

Mutation and deletion analyses of the *PRKAR1A* gene in a CNC family. (A) Scanned segments of sequencing electropherograms of leukocytes (left) and the tumor (right) DNA from the proband. At the top of each panel, nucleotide sequences of WT (black) and a frameshift mutation (red) are indicated. (B) Validation of *PRKAR1A* deletion by qPCR. Upper diagram shows the genomic structure of the *PRKAR1A* gene. The vertical lines indicate positions where DNA copy numbers were measured in introns (Int) 1, 3, 5, and 8 and exon (ex) 11. The graph shows relative DNA copy numbers at each indicated region of the *PRKAR1A* gene compared with the *TBP* gene in leukocytes from the proband (III-2, P), father (II-1, F), and mother (II-2, M) and the tumor (T). The albumin (*ALB*) gene on 4q13.3 was analyzed as a control. A full colour version of this figure is available via http://dx.doi.org/10.1530/EJE-14-0685.